Presented at the 33rd European PV Solar Energy Conference and Exhibition, 24-29 September 2017, Amsterdam, The Netherlands

KEY ASPECTS FOR FABRICATION OF P-TYPE CZ-SI PERC SOLAR CELLS EXCEEDING 22% CONVERSION EFFICIENCY

S. Werner, E. Lohmüller, P. Saint-Cast, J.M. Greulich, J. Weber, S. Schmidt, A. Moldovan, A.A. Brand, T. Dannenberg, S. Mack, S. Wasmer, M. Demant, M. Linse, R. Ackermann, A. Wolf, R. Preu
Fraunhofer Institute for Solar Energy Systems ISE, Heidenhofstr. 2, 79110 Freiburg, Germany
Phone: +49 761 - 4588 5049; e-mail: sabrina.werner@ise.fraunhofer.de

ABSTRACT: This paper gives a close-up insight into recent and future developments that are performed with industrial focus at Fraunhofer ISE's PV-TEC pilot-line to increase the energy conversion efficiency of 6-inch p-type Czochralski-grown silicon (Cz-Si) passivated emitter and rear cells (PERC) to 22% and above. First, the current status of PERC solar cell fabrication allowing for conversion efficiencies up to 21.5% is discussed. Then, we examine four key aspects in detail that need to be considered for optimizing the cells' front side to boost the cell efficiency to the 22% regime. We demonstrate selective emitter laser doping out of the phosphosilicate glass layer, which is formed by a gas phase phosphorus oxychloride diffusion process. After diffusion and wet-chemical emitter etch back, the field emitter features a very low saturation current density of only 31 fA/cm² (textured, SiN_x-passivated). Specific contact resistances of 1 mΩcm^2 confirm the low-resistance contacting of the laser-doped surfaces using a commercially available silver screen printing paste. Apart from developing an accurate alignment procedure to match laser-structured and screen-printed layouts, we have also optimized our single-step screen-printing process for finger widths of 38 µm at 16 µm height. Based on simulations we find that efficiencies up to 22.5% are possible when the optimized process routes are integrated into PERC solar cells.
Keywords: p-type silicon solar cells, PERC, monocrystalline, selective emitter, passivation

1 INTRODUCTION

The passivated emitter and rear cell (PERC) [1] technology on p-type silicon is of very high interest for both research institutes and industry. It has entered mass production during the last years and it is forecast to gain more and more market share [2]. Thus, improving the energy conversion efficiency of PERC solar cells is of major interest for the photovoltaic community. The improvement of the cell's front side is identified as next step to boost the efficiency to 22% and above [3–7]. Lots of research on this subject is performed, but often details regarding the fabrication process or the implementation of novel/adapted processes are not discussed.

The aim of this work is to give a close-up insight into recent and future p-type silicon PERC technology that is being developed with focus on industrial application at Fraunhofer ISE's PV-TEC pilot-line [8]. We discuss in detail the key aspects that need to be considered for a successful integration of necessary process developments into the baseline sequence to target the 22% cell efficiency regime. Therefore, the integration of a selective emitter using laser doping out of the phosphosilicate glass (PSG) layer and several related key aspects to be tackled are discussed, which are expected to have a high impact on future cell development.

2 APPROACH

This paper discusses the improvement of the p-type silicon PERC baseline fabrication process at Fraunhofer ISE's PV-TEC pilot-line [8]. Our continuous process development comprises a two-step approach. First, we characterize and optimize the processes of interest using test samples like, e.g., charge carrier lifetime samples, aluminum back surface field (Al-BSF) solar cells, etc. In a second step, the most promising processes are integrated into the PERC baseline process. Therefore, we examine variations of different processes on the basis of monthly cell runs with 200 wafers each for continuous optimization. The p-type wafer material used is mainly magnetically-cast Czochralski silicon (mCz-Si), as it offers stable high-quality material properties and also features a significantly less pronounced impact of boron-oxygen-related light-induced degradation in comparison with conventional Cz-Si. However, conventional Cz-Si wafers are also used from time to time to benchmark our baseline process.

In 2016, we mainly focused on rear side and base material optimizations while ensuring a stable and reproducible baseline process. As the front side currently limits the efficiency of our PERC solar cells [4], we carried out intensive investigations regarding possible front side optimizations. We identified the following four key aspects to be tackled for a successful fabrication of p-type Cz-Si PERC solar cells with 22% efficiency and above:

(i) The dark saturation current density j_{0e} of the passivated emitter needs to be decreased. Our approach is to decrease the surface doping concentration of the emitter by optimized diffusion processes as well as by adding a wet-chemical emitter etch back process. Additionally, the surface passivation needs to be adapted for such lowly-doped emitters. Also, the dark saturation current density $j_{0e,met}$ of the front screen-printed and fired silver contacts needs to be decreased, while a low specific contact resistance ρ_C must be ensured. Therefore, a selective emitter approach with laser doping out of the PSG layer [9,10] is pursued.

(ii) The process integration of the selective emitter approach including the emitter etch back process into the baseline sequence needs to be realized. For this purpose, we investigate two different process sequences.

(iii) The accurate alignment of the screen-printed grid onto the laser-structured selective emitter needs to be ensured. Therefore, we develop an advanced alignment procedure.

(iv) The front metallization needs to be improved. Different screens and silver pastes are tested to realize smaller finger widths and maintaining high aspect ratios.

All the experiments performed with respect to the mentioned key aspects provide experimentally derived input parameters for simulation-based estimations of the achievable energy conversion efficiencies when the results are transferred into the PERC baseline.

3 PROCESS SEQUENCES

3.1 PERC solar cell fabrication

Fig. 1 shows the recent PERC baseline process at Fraunhofer ISE. The industrial-oriented solar cell fabrication is carried out in the PV-TEC pilot-line [8]. Pseudo-square p-type Cz-Si wafers with an edge length of 156 mm serve as starting material for PERC solar cell fabrication. After alkaline texturing, a tube diffusion using an industrial furnace with phosphorus oxychloride ($POCl_3$) as liquid dopant precursor forms the phosphorus-doped homogeneous emitter. The used $POCl_3$ diffusion is an industrial process that features an in-situ oxidation step and enables full-boat loadings with 200 wafers with sufficient doping uniformity over the single wafers as well as over the entire boat [11]. Subsequently, an inline wet-chemical etching process removes the rear emitter and the front PSG layer.

A wet-chemical cleaning step precedes the surface passivation. The passivation of the rear surface is ensured by a 6 nm-thin aluminum oxide (Al_2O_3) layer deposited by fast atomic layer deposition (fast-ALD), followed by an outgassing step in a tube furnace with N_2 atmosphere and a temperature plateau at 550°C for 10 minutes. Instead of depositing the Al_2O_3 layer by a fast-ALD process, we also have the possibility to deposit this layer by plasma-enhanced chemical vapor deposition (PECVD) using the MAiA system that is wide-spread in industry. In both cases, a minimum 100 nm-thick silicon nitride (SiN_x) layer, deposited by PECVD, serves as capping layer on top of the Al_2O_3 layer. On the front side, a 75 nm-thick non-graded PECVD SiN_x layer serves as anti-reflection coating and surface passivation.

An infrared laser process locally ablates the rear passivation layer stack in order to form the local contact openings (LCO). The front and rear metallization is applied using screen printing processes with commercially available metal pastes. For the front metallization, we perform a double printing step with printing the same layout a second time after paste drying. The front silver grid features five busbars and 100 fingers. The five busbars are tapered with an effective busbar width $w_{busbar,eff}$ = 400 µm over the total busbar length. The finger width w_{finger} after contact firing is measured to be $w_{finger} \approx 55$ µm. The rear electrode consists of full-area aluminum and optional silver solder pads. Finally, contact firing with varying the peak temperature is performed in an industrial conveyor belt furnace.

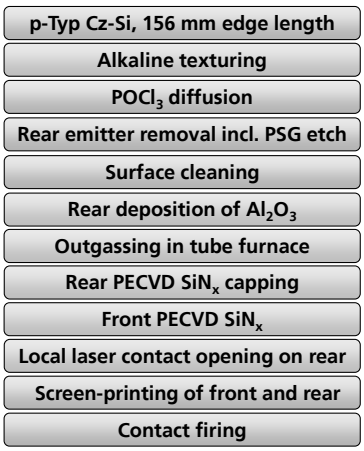

Figure 1: Recent p-type Cz-Si PERC baseline fabrication process at Fraunhofer ISE.

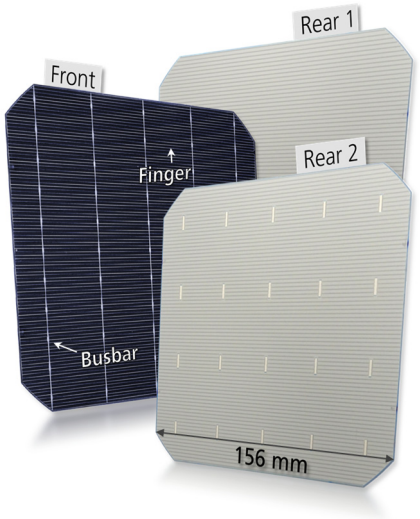

Figure 2: Photograph of a p-type Cz-Si PERC solar cell from the front and the rear side fabricated at Fraunhofer ISE's PV-TEC pilot-line (Rear 1: w/o solder pads, Rear 2: with solder pads).

Fig. 2 shows the front and rear side cell design of our PERC solar cells with line-shaped rear side contacts. The rear side "Rear 2" shows the silver solder pads, which allow the integration of the PERC solar cells into modules.

3.2 Test samples and characterization methods

All j_{0e} values given in this work are determined from quasi-steady-state photoconductance (QSSPC) measurements on symmetric n-type Cz-Si lifetime samples with high base resistivity. Their surfaces are alkaline textured. Although these samples do not feature an Al_2O_3 passivation layer, an outgassing step is performed to resemble the cell fabrication process (see Fig. 1). Then, the front and rear surfaces are passivated by a conventional SiN_x layer. A firing step activates the passivation properties. For evaluation of the QSSPC measurements, the procedure from Ref. [12] is used.

Charge carrier concentration profiles after PSG removal are obtained using the electrochemical capacitance-voltage (ECV) technique. The surface roughness needs to be taken into account as the samples are initially alkaline textured and partly treated by a laser process. The measured charge carrier concentration profiles are corrected to match the sheet resistance R_{sh} by applying the procedure described in Ref. [13]. For this end, four point probe measurements determine the emitter sheet resistance R_{sh} in the region of interest.

To determine specific contact resistances ρ_C, measurements according to the transfer length method (TLM) [14] are performed. The investigated samples undergo alkaline texturing, $POCl_3$ diffusion, optional laser doping, PSG etching, PECVD SiN_x passivation, screen-printing, and finally, contact firing. The screen-printing layout is the same as that used for the solar cells.

4 EFFICIENCY IMPROVEMENTS IN 2016

The conversion efficiency η improvements for PERC solar cells during the year 2016 are depicted in Fig. 3. Starting with a mean value of η_{mean} = 20.8% in January 2016, the efficiency increases to η_{mean} = 21.3% ensuring a stable and reproducible baseline process. The champion

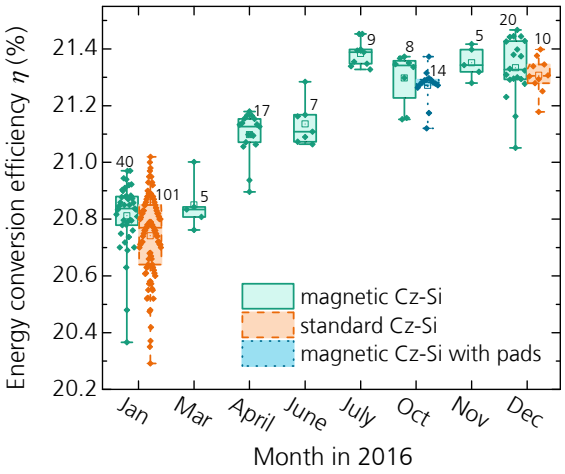

Figure 3: Improvement in conversion efficiency η of PERC solar cells fabricated at Fraunhofer ISE's PV-TEC pilot-line in 2016 for different materials, without or with solder pads. Per experiment, only the most efficient parameter set is shown. All measurements are performed with an industrial cell tester in the "as processed" state. The numbers given above the box plots state the total number of PERC solar cells fabricated within the respective process group.

cell shows $\eta = 21.5\%$ with open-circuit voltage V_{OC} = 665 mV, short-circuit current j_{SC} = 39.7 mA/cm^2, and fill factor $FF = 81.2\%$ in the as-processed state (in-house measurement). Our baseline is also compatible with standard Cz-Si material, which performs similar to the mCz-Si wafers (see Fig. 3: January [15] and December). Another experiment (see October) shows the successful integration of silver solder pads with similar $\eta_{mean} = 21.3\%$ for PERC cells either with or without solder pads. In adhesion tests of the front grid and the rear pads, cell breakage confirms sufficient adhesion and thus the module-readiness of our PERC cells.

The following process adaptions/optimizations are the main changes for the achieved efficiency improvements in Fig. 3:

- January to March: change in base resistivity and LCO line pitch
- March to April: evaluation of new aluminum pastes
- April to June: change in LCO line pitch
- June to July: change in base resistivity
- July to October: change in LCO line pitch and implementation of silver solder pads
- October to November: adaption of the rear LCO geometry from lines to dots by increasing the laser pulse distance and adapting the aluminum paste
- November to December: process simplification, i.e., the omission of a wet-chemical rear side polishing step that, until then, has preceded $POCl_3$ diffusion. Simultaneously, an alkaline texturing process resulting in smaller pyramids is implemented.

In addition to these main adjustments, numerous smaller optimizations—that are difficult to quantify—are also incorporated in the continuously evolving fabrication process.

5 KEY ASPECTS FOR INCREASING THE EFFICIENCY OF PERC SOLAR CELLS TO 22% AND ABOVE

In the PERC cell runs in 2016, we mainly focused on rear side and base material optimizations. In parallel experiments that are based on test samples or Al-BSF solar cells, intensive investigations have been carried out separately in order to optimize the front side processes.

5.1 Key aspect one: Lower emitter dark saturation current density

The currently used homogeneous phosphorus emitter with $R_{sh} \approx 90\ \Omega$/sq allows for $j_{0e} \approx 85$ fA/cm^2 on alkaline textured surface passivated by a non-graded PECVD SiN_x layer [11]. An approach to reduce j_{0e} of the passivated diffused regions (i.e. to increase the V_{OC}) is the reduction of the phosphorus doping concentration at the silicon surface N_{surf} [16]. We showed the successful low-resistive electrical contacting of very lightly phosphorus-doped surfaces with $N_{surf} \approx 3 \cdot 10^{19}$ cm^{-3} with low specific contact resistances $\rho_C \approx 5$ mΩcm^2 for a commercial state-of-the-art silver screen-printing paste [13]. On symmetric lifetime samples with alkaline textured surfaces and PECVD SiN_x passivation layer, we achieve very low $j_{0e} \approx 40$ fA/cm^2 for these emitters with low N_{surf} if the samples undergo the outgassing step before SiN_x layer deposition. We assume that despite the inert atmosphere, a thin passivating silicon dioxide (SiO_2) layer grows on the emitter surface during the outgassing step and improves the surface properties.

Based on these promising findings, we implemented homogenous emitters with low N_{surf} in Al-BSF solar cells. However, the solar cells with these lowly-doped emitters do not show a performance advantage compared to the solar cells with the reference emitter featuring $N_{surf} \approx 1.2 \cdot 10^{20}$ cm^{-3}. This is caused by a lower V_{OC} due to significant larger $j_{0e,met}$ below the silver contacts for the lowly-doped emitter groups [13].

Thus, the novel emitters are very promising in terms of ρ_C and j_{0e}, but still challenging in terms of contact recombination $j_{0e,met}$. Whenever new generations of silver screen printing pastes allow for lower $j_{0e,met}$, these emitters are very interesting for further development using homogenous emitter diffusion.

Until then, a selective emitter is advantageous to decrease $j_{0e,met}$ for the front screen-printed and fired silver contacts, while ensuring low ρ_C, as higher doping underneath the metal contacts significantly reduces $j_{0e,met}$ [17]. Our approach to form a selective emitter in the areas of the metal contacts is local laser doping out of the PSG layer [9,10], as it is highly industrial relevant.

The PSG layer grown during $POCl_3$ diffusion must provide a sufficient amount of phosphorus atoms for local laser doping. On the other hand, N_{surf} in the photoactive area must not be too high to allow for low j_{0e}. Our approach for a $POCl_3$ diffusion process that takes both requirements into account is the use of a moderate deposition at the beginning to allow for low N_{surf} and the addition of a second deposition step with active nitrogen (N_2) flow through the $POCl_3$ bubbler after the drive-in step to provide a PSG layer with high phosphorus concentration [18,19]. The second deposition step is intended to not change the doping profile any further [18,19].

Fig. 4 shows the resulting as-diffused doping profile on alkaline textured surface after PSG removal for this $POCl_3$ diffusion ($R_{sh} \approx 116\ \Omega$/sq, $N_{surf} \approx 5.7 \cdot 10^{19}$ cm^{-3}).

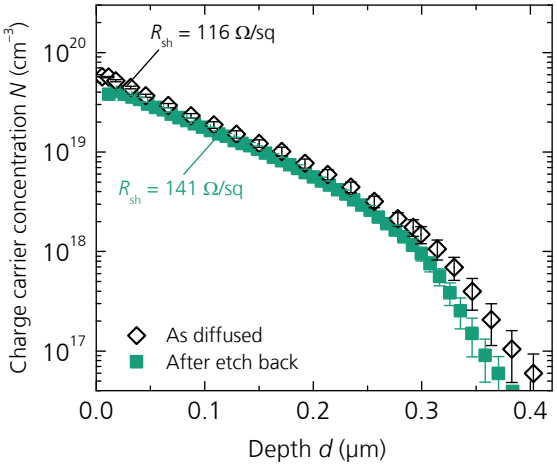

Figure 4: Charge carrier concentration profiles measured by ECV technique after PSG etching (as diffused) and after emitter etch back on alkaline textured surface. The sheet resistances R_{sh} are given.

For symmetric alkaline textured lifetime samples featuring this emitter, j_{0e} is found to be $j_{0e} = (42 \pm 2)$ fA/cm².

To further reduce the emitter recombination in the photoactive area, the emitter is partly etched back in solutions of either hydrofluoric acid (HF) and persulfate [20] or ozone [21], which leads to an increase in R_{sh}. We target a value of 140 Ω/sq ≤ R_{sh} ≤ 150 Ω/sq such that the lateral conductivity is not decreased too much for our current grid layout. Fig. 4 illustrates the doping profile of the etched-back emitter with $R_{sh} \approx 141$ Ω/sq and $N_{surf} \approx 3.8 \cdot 10^{19}$ cm^{-3}. By comparison with the as-diffused profile, the profile after etch back is shifted by approx. 20 nm, which corresponds to the silicon removal at the emitter surface. We find $j_{0e} = (31 \pm 4)$ fA/cm² for this etched-back emitter.

For the laser doping experiments, we use a pulsed ultraviolet laser with a wavelength $\lambda = 355$ nm [10]. As previously, also symmetrically alkaline textured and diffused carrier lifetime samples are utilized for the examinations. To determine R_{sh}, the saturation current density $j_{0e,laser}$, and ρ_C for the laser-structured areas, test fields are formed either on one or both wafer sides by applying different laser parameters A-D (i.e., different pulse energies, pulse pitches and line pitches).

Fig. 5 shows an excerpt of the obtained results for the laser-doped test fields in terms of $j_{0e,laser}$ and ρ_C in dependence of R_{sh}. For comparison, the result of the etched-back emitter without laser doping is also plotted ("Ref"). The laser processed fields exhibit moderate recombination current densities 125 fA/cm² < $j_{0e,laser}$ < 280 fA/cm² with 80 Ω/sq > R_{sh} > 40 Ω/sq for the different applied laser parameters. Specific contact resistances 1 mΩcm² ≤ ρ_C < 4 mΩcm² prove the low-resistance electrical contacting of these laser-doped regions compared to $\rho_C \approx 650$ mΩcm² when laser-doping is not applied.

Fig. 6 shows the corresponding charge carrier concentration profiles after laser doping and PSG removal. Obviously, the laser processing yields significant higher charge carrier concentrations in the course of the profile compared to the reference profile after etch back. The surface concentration increases significantly from initially $N_{surf} \approx 3.8 \cdot 10^{19}$ cm^{-3} after etch back to a surface-near maximum carrier concentration (A) $N_{max} \approx 5.0 \cdot 10^{19}$ cm^{-3}, (B) $N_{max} \approx 6.0 \cdot 10^{19}$ cm^{-3}, (C) $N_{max} \approx 8.0 \cdot 10^{19}$ cm^{-3}, and (D) $N_{max} \approx 1.1 \cdot 10^{20}$ cm^{-3}.

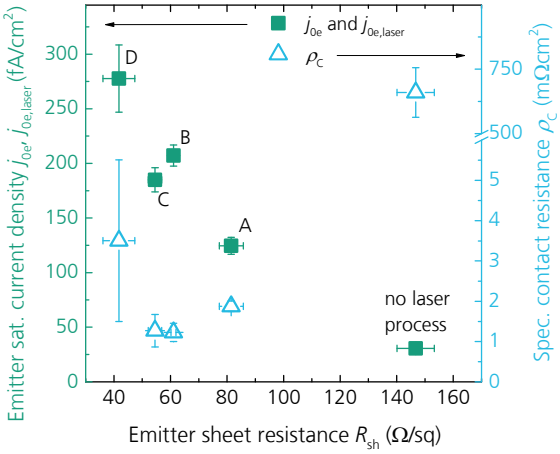

Figure 5: Emitter saturation current densities j_{0e} and $j_{0e,laser}$ for the photoactive and laser-doped areas, respectively (initially textured, SiN_x-passivated, fired), and specific contact resistance ρ_C in dependence on the emitter sheet resistance R_{sh} for different laser doping processes A-D (variation of power, pulse pitch, and line pitch). The reference "Ref" without laser doping is also shown. All samples have been diffused in the same $POCl_3$ diffusion process and etched back in HF and persulfate (compare Fig. 4).

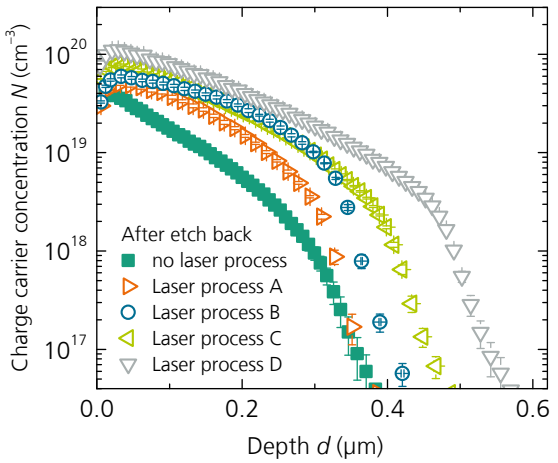

Figure 6: Charge carrier concentration profiles measured by the ECV technique after laser processes A-D and wet-chemical etch back. The profile after etch back from Fig. 4 is shown as reference.

5.2 Key aspect two: Process integration of the emitter etch back step into the PERC baseline

The process integration of the selective emitter approach with respect to the etch back process is another key aspect. For the emitter etch back, there are two options for its implementation into the fabrication sequence.

First, it might be integrated after wet-chemical removal of the rear emitter before surface passivation. At this stage, the doping-type on front and rear side of the wafers is different. In this case we found that R_{sh} does not change significantly during etching. The cause probably lies in the so-called "cathodic protection": the n-doped front is protected from the etching solution and prevents the removal of a significant amount of silicon at the emitter surface.

The second option is to implement the etch back before rear emitter removal. In doing so, the PSG layers on

front and rear side are also etched. This is important because these PSG layers usually ensure high wettability of the front side of the wafers with the water film sprayed onto it before rear emitter removal. The water film protects the front emitter from possible wrap-around of the etching solution and gas phase etching. Hence, when no emitter etch back is performed, the water sticks to the front side as the PSG layer is hydrophilic. The PSG layer of the front side is then etched after rear emitter removal in HF within the same inline wet-chemistry tool.

In our case, however, the emitter etch back precedes the rear emitter removal and thus, no PSG layer is present on the front side during the latter. Hence, the front side is hydrophobic and not able to hold the protective water film. To solve this, we grow a thin wet-chemical SiO_2 layer in an ozone-based solution at the end of the emitter etch back. This SiO_2 layer provides a hydrophilic front surface during rear emitter removal.

We tested this approach on PERC cells with homogenous emitter without noticing occurring wrap-around as a variation in the experiment from November 2016 (see Fig. 3). These PERC cells are fabricated according to an adapted process sequence compared to Fig. 1, including the PSG layer removal and the SiO_2 layer growth in ozone-based solution after $POCl_3$ diffusion before rear emitter removal. The measured mean energy conversion efficiency $\eta_{mean} = 21.3\%$ for these cells is similar to the cells of the reference group, which are fabricated according to the standard sequence for homogeneous emitter cells.

5.3 Key aspect three: Accurate alignment of the screen-printed grid onto the laser-structured selective emitter

A further key aspect is a high alignment precision of the screen-printed grid on top of the laser-structured selective emitter. If misalignment occurs, as illustrated in Fig. 7, this will cause significant losses in *FF* as no low-resistive electrical contact can be formed to the adjacent etched-back emitter. Additional losses in V_{OC} will occur due to high recombination in these not well-shielded, metallized areas. Losses in short-circuit current j_{SC} will arise as the laser-doped area that is not covered by the metal fingers yields a higher reflectivity and reduced short-wavelength short-circuit current density. Hence, it is very important to align screen printing and laser processes very precisely.

We developed an alignment procedure that considers inaccuracies of laser and screen printing processes such as screen warping. The result is an adapted laser grid that resembles the actual screen-printed grid. This procedure has already been successfully tested on so-called "pPassDop" solar cells in Ref. [22]. We demonstrated an accurate alignment of 65 µm-wide fingers on 37 µm-wide laser-processed lines over the whole wafer for the rear side metallization of these "pPassDop" solar cells.

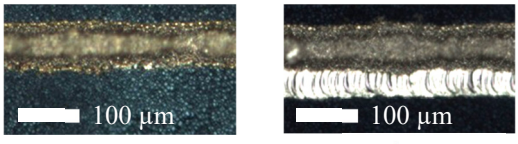

(a) (b)

Figure 7: Light-micrographs of a silver finger on a wafer for which the alignment procedure (a) was applied or (b) was not. The bright laser-doped line is only visible in (b) since it is completely covered by the silver finger in (a). The images are taken from Ref. [22].

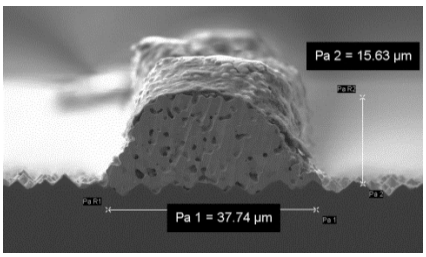

Figure 8: Scanning electron micrograph image of a cross section of a screen-printed and fired finger using a commercially available silver paste.

5.4 Key aspect four: Smaller front side finger widths

The last key aspect discussed in this paper is the front metallization. From an actual measured finger width after contact firing $w_{finger} \approx 55$ µm, we aim to significantly reduce w_{finger}. Therefore, we examined screens and silver pastes from different suppliers. We found a promising new combination of screen mesh and commercially available silver paste that allows for printing shallower fingers. Fig. 8 shows a scanning electron micrograph of a screen-printed and fired silver finger with significantly reduced width of $w_{finger} \approx 38$ µm and a finger height of $h_{finger} \approx 16$ µm resulting from a single printing step. Due to the improved aspect ratio by using a new generation commercially-available silver screen-printing paste, the grid resistance (60 Ω/m per finger) does not change compared to our current 55 µm-wide finger contacts that are formed by double-printing. With the lower finger width and the increased R_{sh} between the contacts when using the selective emitter from section 5.2, the finger number needs to be increased. This increase avoids *FF* losses due to the reduced lateral conductivity in this emitter. An estimation using the software tool GridMaster [23] reveals that the amount of fingers needs to be increased to a number between 110 and 120.

6 SIMULATION RESULTS AND NEXT STEPS

6.1 Simulation of conversion efficiency

All findings concerning the four key aspects discussed in the sections 5.1 to 5.4 are important for increasing the efficiency of our PERC solar cells. With fast metamodeling of numerical device simulations [24], we can easily estimate the cell efficiency potential when implementing the discussed improvements in the form of experimentally derived input parameters.

We integrate a selective emitter to the simulation of the latest PERC solar cells with homogeneous emitter from the experiment in December in Fig. 3. As $j_{0e,met}$ is not determined experimentally, we vary $j_{0e,met}$ for the simulation with values of $j_{0e,met} = \{1000$ fA/cm², 500 fA/cm², 200 fA/cm²$\}$; see also Table 1. The finger number is optimized accordingly in terms of leveling

Table 1: Simulated η for different $j_{0e,met}$ and optimized finger number. The total saturation current density $j_{0,front}$ of the front side is also stated.

$j_{0e,met}$ (fA/cm²)	Finger number	$j_{0,front}$ (fA/cm²)	η (%)
1000	112	73	22.2
500	116	52	22.4
200	120	39	22.5

shading and contact recombination with series resistance losses.

As result of the simulations, the total saturation current density $j_{0,front}$ of the front side is found to be between 39 fA/cm² ≤ $j_{0,front}$ ≤ 73 fA/cm², see also Table I. This is a significant improvement compared to our current PERC solar cells with $j_{0,front}$ = 152 fA/cm². The conversion efficiencies are computed to values in a range of 22.2% ≤ η ≤ 22.5% for the given $j_{0,front}$. Thus, the simulations clearly show the potential of our performed optimizations and forecast PERC solar cells with efficiencies exceeding 22% after integration of the discussed adaptions from the sections 5.2 to 5.4 into the "new" baseline sequence for selective emitter solar cells.

6.2 PERC solar cells in 2017

After all the preliminary work performed in 2016 as discussed above, we have been ready to implement the developed processes for the selective emitter into a full cell fabrication sequence. This was started in the beginning of 2017. Unfortunately, the running experiment has been lost due to a fire in our PV-TEC laboratory on February 24th, 2017 [25]. Not only have the respective samples been destroyed, but also all other industrial tools for PERC solar cell fabrication that have been located in this laboratory. Thus, the implementation of the selective emitter into fully fabricated PERC solar cells has not been performed yet.

As we have access to other labs and tools at Fraunhofer ISE that are capable to process large-area PERC solar cells, we have been able to re-establish a PERC baseline process in the meantime. We transferred our standard processes from the PV-TEC tools to these interim machines as far as possible. To date, we are again able to fabricate PERC solar cells according to the fabrication sequence shown in Fig. 1 with current peak energy conversion efficiencies of η = 20.9%.

6.3 Outlook to 2018

At the end of the first quarter of 2018, we plan to launch the operation of the PV-TEC laboratory again. New and up-to-date industrial equipment for the frontend processes until passivation will be located in our PV-TEC cleanroom laboratory for industrial equipment [26], while the also new and up-to-date industrial backend equipment will be located in the rebuilt PV-TEC. After the hook-up of the new machines, we will again pick up the above discussed developments and aim at their implementation into PERC solar cells with selective emitter.

7 SUMMARY

Our industrial-oriented PERC baseline process showed stable and reproducible results for 6-inch p-type Cz-Si PERC solar cells achieving mean energy conversion efficiencies η_{mean} = 21.3% and η = 21.5% for the champion cell before the fire in February 2017. Currently, after transferring processes, our baseline achieves 20.9% peak efficiencies. Prior to the fire accident, the cells' front side was identified to be the limiting factor on the way to 22% cell efficiency to date. To improve the cell's front side, we investigated the approach to incorporate a selective emitter using laser doping from the PSG layer into our baseline process. This implementation of a selective emitter and the 22%-efficiency target induces four key aspects:

(i) We show the reduction of the surface doping concentration of the emitter in the photoactive region by an adapted $POCl_3$ diffusion process and a subsequent wet-chemical emitter etch back step. In doing so, we are able to decrease the emitter dark saturation current density to $j_{0e} \approx (31 \pm 4)$ fA/cm² on alkaline textured surface passivated with a standard, non-graded PECVD SiN_x layer.

A high phosphorus concentration within the PSG layer for laser doping is ensured by the above mentioned $POCl_3$ diffusion process that features a second deposition step with active N_2 flow through the $POCl_3$ bubbler after drive-in. For the laser-doped region, we find the emitter dark saturation current density to be $j_{0e,laser} \approx 180$ fA/cm² (SiN_x passivated, fired) with a sheet resistance of $R_{sh} \approx$ 54 Ω/sq. Specific contact resistances of $\rho_C \approx 1$ mΩcm² confirm low-resistive electrical contacting after firing using a commercially available silver screen printing paste.

(ii) Concerning process integration, we identify that the emitter etch back needs to be performed before rear emitter removal.

(iii) An accurate alignment of the screen-printed grid on top of the laser-structured selective emitter is crucial for avoiding losses in η. We developed a procedure that considers inaccuracies of laser and screen-printing processes such as screen warping.

(iv) We optimized our screen-printing processes now allowing for a finger width $w_{finger} \approx 37$ µm at a finger height $h_{finger} \approx 16$ µm after single printing.

Simulations that are based on the experimentally derived input parameters from this work imply efficiencies up to 22.5% for 6-inch p-type Cz-Si PERC solar cells when the mentioned optimized processes are integrated into the "new" baseline PERC process for selective emitter solar cells at Fraunhofer ISE.

ACKNOWLEDGEMENTS

The authors would like to thank all colleagues at the Fraunhofer ISE PV-TEC for their teamwork and J. Horzel for his support and the fruitful discussions. This work was funded by the German Federal Ministry for Economic Affairs and Energy mainly within the research projects "CUT A" (contract no. 0325823), "POLDI" (contract no. 0324079D), "HELENE" (contract no. 0325777D), "Groschen" (contract no. 0324012B), "AdmMo" (contract no. 0325775E), "CUT B" (contract no. 0325910A).

REFERENCES

[1] A. W. Blakers, A. Wang, A. M. Milne et al., "22.8% efficient silicon solar cell", *Appl. Phys. Lett.*, vol. 55, no. 13, pp. 1363–1365, 1989.

[2] ITRPV, 2017, "International Technology Roadmap for Photovoltaic (ITRPV) - Results 2016", available onl.: http://www.itrpv.net/Reports/ Downloads/2017/.

[3] B. Min, H. Wagner, M. Müller et al., "Incremental efficiency improvements of mass-produced PERC cells up to 24%, predicted solely with continuous development of existing technologies and wafer materials", *Proc. 31st EU PVSEC*, Hamburg, Germany, 2015, pp. 473–476.

[4] P. Saint-Cast, S. Werner, J. Greulich et al., "Analysis of the losses of industrial-type PERC solar cells", *Phys. Status Solidi A*, 2016.

[5] R. Brendel, T. Dullweber, R. Peibst et al., "Breakdown of the efficiency gap to 29% based on experimental input data and modeling", *Prog. Photovolt: Res. Appl.*, vol. 24, no. 12, pp. 1475–1486, 2016.

[6] W. Deng, F. Ye, R. Liu et al., "22.61% efficient fully screen printed PERC solar cell", *Proc. 44th IEEE PVSC*, Washington D.C., USA, 2017.

[7] M. Müller, B. Bitnar, G. Fischer et al., "Loss analysis of 22% efficient industrial PERC solar cells", *Energy Proced.*, in press, 2017.

[8] D. Biro, R. Preu, S. W. Glunz et al., "PV-TEC: Photovoltaic technology evaluation center - design and implementation of a production research unit", *Proc. 21st EU PVSEC*, Dresden, Germany, 2006, pp. 621–624.

[9] L. Ventura, A. Slaoui, J. C. Muller, "Realization of selective emitters by rapid thermal and laser assisted techniques", *Proc. 13th EU PVSEC*, Nice, France, 1995, pp. 1578–1581.

[10] U. Jäger, S. Mack, C. Wufka et al., "Benefit of selective emitters for p-type silicon solar cells with passivated surfaces", *IEEE J. Photovoltaics*, vol. 3, no. 2, pp. 621–627, 2013.

[11] S. Werner, E. Lohmüller, S. Maier et al., "Process optimization for the front side of p-type silicon solar cells", *Proc. 29th EU PVSEC*, Amsterdam, The Netherlands, 2014, pp. 1342–1347.

[12] A. Kimmerle, J. Greulich, A. Wolf, "Carrier-diffusion corrected J_0-analysis of charge carrier lifetime measurements for increased consistency", *Sol. Energy Mater. Sol. Cells*, vol. 142, pp. 116–122, 2015.

[13] S. Werner, E. Lohmüller, S. Maier et al., "Challenges for lowly-doped phosphorus emitters in silicon solar cells with screen-printed silver contacts", *Energy Proced.*, in press, 2017.

[14] H. H. Berger, "Contact resistance and contact resistivity", *J. Electrochem. Soc.*, vol. 119, no. 4, pp. 507–514, 1972.

[15] P. Saint-Cast, I. Reis, J. Greulich et al., "Cz silicon benchmark for p-type PERC solar cells", *Proc. 32nd EU PVSEC*, Munich, Germany, 2016, pp. 1038–1043.

[16] A. Wolf, A. Kimmerle, S. Werner et al., "Status and perspective of emitter formation by $POCl_3$-diffusion", *Proc. 31st EU PVSEC*, Hamburg, Germany, 2015, pp. 414–419.

[17] T. Fellmeth, A. Born, A. Kimmerle et al., "Recombination at metal-emitter interfaces of front contact technologies for highly efficient silicon solar cells", *Energy Proced.*, vol. 8, pp. 115–121, 2011.

[18] S. Werner, S. Mourad, W. Hasan et al., "Structure and composition of phosphosilicate glass systems formed by $POCl_3$ diffusion", *Energy Proced.*, in press, 2017.

[19] S. Werner, E. Lohmüller, J. Weber et al., "Suitability of low recombinative $POCl_3$ diffusion processes with in-situ oxidation for forming laser-doped selective emitters", *Proc. 33rd EU PVSEC*, Amsterdam, The Netherlands, 2017.

[20] A. Lachowicz, K. Ramspeck, P. Roth et al., "Nox-free solution for emitter etch-back", *Proc. 27th EU PVSEC*, Frankfurt, Germany, 2012, pp. 1846–1850.

[21] A. Moldovan, K. Birmann, J. Rentsch et al., "Combined ozone/HF/HCl based cleaning and adjusted emitter etch-back for silicon solar cells", *Solid State Phenomena*, vol. 195, pp. 305–309, 2013.

[22] E. Lohmüller, S. Werner, M. H. Norouzi et al., "Bifacial p-type PERL solar cells with screen-printed pure Ag metallization and 89% bifaciality", *Proc. 33rd EU PVSEC*, Amsterdam, The Netherlands, 2017.

[23] T. Fellmeth, F. Clement, D. Biro, "Analytical modeling of industrial-related silicon solar cells", *IEEE J. Photovoltaics*, vol. 4, no. 1, pp. 504–513, 2014.

[24] S. Wasmer, A. A. Brand, J. M. Greulich, "Metamodeling of numerical device simulations to rapidly create efficiency optimization roadmaps of monocrystalline silicon PERC cells", *Energy Proced.*, in press, 2017.

[25] Fraunhofer ISE (press release), , "Fraunhofer ISE Laborbrand", available online: https://www.ise.fraunhofer.de/de/presse-und-medien/news/2017/brand-in-labor-im-solar-info-center.html, accessed on: 09-21-2017.

[26] J. Rentsch, A. Moldovan, M. Bivour et al., "A new pilot research facility for HJT and selective contact solar cells – PV-TEC SELECT", *Proc. 33rd EU PVSEC*, Amsterdam, The Netherlands, 2017.